Hindawi
Advances in Meteorology
Volume 2022, Article ID 7206137, 16 pages
https://doi.org/10.1155/2022/7206137

Research Article

Variation in the Positioning of the Asian Summer Monsoon Boundary in the Tibetan Plateau and Potential Drivers

Jie Li,[1] **Liya Jin**,[1,2] **Jinjian Li**,[1] **Zeyu Zheng**,[2] **and Zhitao Yan**[1]

[1]*School of Atmospheric Sciences, Chengdu University of Information Technology, Chengdu 610225, China*
[2]*College of Earth and Environmental Sciences, Lanzhou University, Lanzhou 730000, China*

Correspondence should be addressed to Liya Jin; jinly@cuit.edu.cn

Received 31 October 2021; Accepted 29 March 2022; Published 30 April 2022

Academic Editor: Panagiotis Nastos

Studying the variation in the boundary position of the Asian summer monsoon in the Tibetan Plateau (TP) region and its potential drivers is important for understanding the climate in this region. Three sets of mean monthly precipitation data from 1980 to 2019 were sourced from the Global Precipitation Climatology Centre, the Climate Research Unit, and China Meteorological Information Service Centre. Several indicators that represent the Asian summer monsoon boundary (ASMB) were selected to compare their applicability to the TP region and elucidate the changes in the location of the ASMB in the TP over the last four decades. The results showed that the ASMB in the TP region extends in a southwest-northeast direction, with a clear north-south variation. It reaches as far north as the Kunlun Mountains and as far south as the Himalayas. The largest amplitude in spatial fluctuation occurs in the middle of the TP, and the smallest amplitude occurs at both ends of the region. A "small-large-small" fluctuation pattern was observed from west to east. The water vapor mainly originates from the South Asian region. The South Asian summer monsoon can move the ASMB position northward, whereas the westerly wind moves the ASMB position southward. Variation in the ASMB in the TP region is closely associated with the South Asian monsoon and westerly wind.

1. Introduction

Monsoons have long been a popular topic of research in the meteorological community. The modern concept of monsoons was introduced as early as the late 17th century, by Halley [1], who argued that they are caused by differences in the heating of the ocean and land by the sun, which, consequently, lead to differences in atmospheric pressure. Later, Hadley [2] extended the monsoon model, whereby the rotation effect of the earth causes the airflow to be affected by the Coriolis force, deflecting it to the right to form a southwesterly wind. The concept of "global monsoon" (GM) has been introduced and improved through observations at different levels and in-depth studies in recent 20 years. "GM" studies have evolved from evaluating regional climate phenomena to investigating global scale effects [3], opening a new phase of research on monsoon precipitation and regions exposed to monsoons [4–7].

The Asian summer monsoon (ASM) is an important part of the GM system. It is the leading climate phenomenon and the main cause of precipitation in Asia [8–10]. Changes to the intensity of the ASM affect this region, including how rainbands are distributed, which may lead to meteorological disasters, such as flooding, under precipitation anomalies [11–13]. On the TP, the precipitation is less than that in the core areas of Asia, such as the East and South Asian area; therefore, the precipitation in the region varies considerably, which, in turn, impacts the vegetation and ecology along the monsoon boundary, and it is also more sensitive to the climate at the edge of the ASM [14–18]. Thus, there is a need to assess how ASMB in the TP changed in the past four decades to better understand the climatic characteristics of TP and GM.

Extensive efforts have been undertaken to delineate the boundary of the monsoon. Previously, the "boundary" was called the northern edge zone of the monsoon, with thermal and dynamic factors being used to monitor how the position

of the monsoon boundary changes. For example, Wang et al. [19] defined the monsoon boundary as areas with southwesterly winds >2.0 ms^{-1}, pseudo-equivalent potential temperature (θse) south of 30°N greater than 340 K, and θse north of 30°N greater than 335 K. Wu et al. [20] defined the monsoon boundary as five-day mean southwesterly winds at 850 hPa and southerly winds >3.0 ms^{-1}, and a five-day mean θse at 850 hPa greater than 335 K. However, the monsoon boundary varies greatly depending on the indicators used to define it. Because the summer monsoon carries a large amount of water vapor, the monsoon boundary could also be defined based on precipitation indicators including annual precipitation of 300–500 mm [21], five-day average precipitation [22], or 20 mm isoline of precipitation variance during summer (June–August) [23]. Additionally, the boundary can be directly delineated from the standardized precipitation indicator, by establishing areas with a difference of 2.0 mm day^{-1} between summer and winter precipitation and more than 55% of summer precipitation as monsoon zones [24], and using the 2.0 mm day^{-1} isoline of summer (May–September) precipitation to determine a northern monsoon boundary indicator [25]. However, defining the monsoon boundary index using kinetic or thermodynamic indicators could have limitations, due to the large topographic effect of the TP [26], with precipitation data possibly being more informative. In this study, we compared the monsoon boundary index by using monthly mean precipitation data and explored its applicability in the TP. We expect that our results will provide new insights on the spatial and temporal fluctuations of the monsoon boundary, and possible factors affecting its location.

2. Data and Methods

2.1. Study Area and Data. The TP (26–40°N and 73–104°E) is the highest plateau in the world, with an average elevation of >4500 m [27]. The TP is located to the south of the southern edge of the Himalayas, north of the Kunlun and Qilian Mountains, west to the Pamir Plateau, and east and northeast to the western section of the Qinling Mountains; it has a total area of approximately 2.5 million km^2 [28] (see Figure 1).

Three different monthly precipitation datasets covering the period from 1980 to 2019 were used in this study. The first dataset was obtained from the Global Precipitation Climatology Centre (GPCC) [29], with a horizontal resolution of 0.5° × 0.5°longitude. The second dataset was obtained from the China Meteorological Data Service Centre, providing monthly precipitation data of China's surface precipitation (CN05) [30], with a horizontal resolution of 0.25° × 0.25°. The third dataset was obtained from the Climate Research Unit (CRU) [31, 32], which provided monthly precipitation data at a horizontal resolution of 0.5° × 0.5°. Monthly wind data were obtained from the monthly reanalyzed data of the National Center for Environmental Prediction/Atmospheric Research (NCEP/NCAR) [33], with a horizontal resolution of 2.5° × 2.5°. The surface wind field was based on reanalyzed monthly values of era5-land monthly averaged data from 1980 to 2019, with a horizontal resolution of 0.1° × 0.1° [34]. Water vapor flux was calculated from era5 monthly averaged pressure data from 1980 to 2019, with a horizontal resolution of 0.25° × 0.25° and a vertical resolution of 37 layers [35]. Land cover type data were obtained from MODerate Resolution Imaging Spectroradiometer (MODIS) data from October 2000 to October 2001, with a horizontal resolution of 0.25° × 0.25°, in which the 17 land cover classification schemes were used based on the International Geosphere-Biosphere Program (IGBP) [36].

2.2. Methods. To assess the interannual and interdecadal variability of the ASMB, we first used time series analysis, discussed its subregional variability, and subsequently employed wavelet analysis to identify its multiple cycles of variability, reflecting the trends at different time scales. To better understand the corresponding dynamic mechanisms or external forcing, composite analysis was used to discuss the wind field at 500 hPa [37, 38] and also calculate the water vapor flux on the TP and its surrounding areas [39–41]. The westerly wind index and the South Asian monsoon index were used to represent the intensity variation of the westerly wind and the South Asian monsoon. The cross wavelets were used to analyze the relationship between the westerly wind-ASMB and the South Asian monsoon-ASMB [42, 43]. The functions and their corresponding definitions are detailed below.

2.2.1. Wavelet Analysis. We selected the Morlet wavelet [44] to analyze the relationship between the South Asian monsoon-monsoon boundary-westerly winds. The Morlet wavelet function is expressed as

$$\Psi(t) = e^{-i\omega_0 t} e^{\left(-t^2/2\right)}, \tag{1}$$

where $\Psi(t)$ is the wavelet function; i is the imaginary symbol of a complex number; and ω_0 is the nondimensional frequency. The Morlet wavelet transform coefficients $W_x(a,b)$ are defined as

$$W_x = (a,b) = C_x(a,b)C_x^*(a,b) = \left|C_x(a,b)\right|^2, \tag{2}$$

where $C_x(a,b)$ and $C_x^*(a,b)$ are the wavelet coefficients of the original and conjugate functions, respectively, of x; a and b represent the time scale and time position factors, respectively. The magnitude of the mode of the Morlet wavelet coefficient of variation indicates the strength of the signal of the characteristic time scale; the real part indicates the information of the distribution and the bit phase of different characteristic time scales at different times. The wavelet variance can be obtained by integrating the squares of all wavelet coefficients for different scales. The wavelet variance can indicate the strength of the fluctuation of that cycle in the time series and is defined as

$$\mathrm{Var}(a) = \int_{-\infty}^{+\infty} \left|C_x(a,b)\right|^2 \mathrm{db}. \tag{3}$$

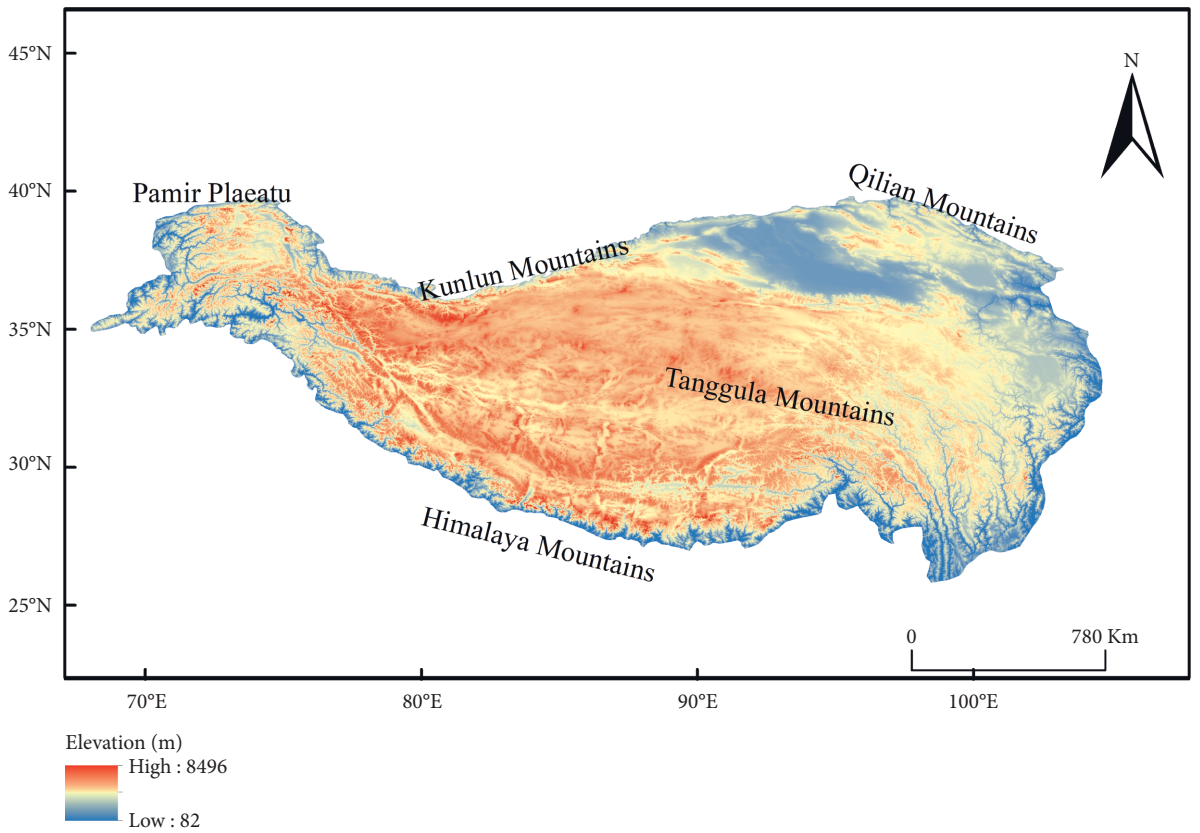

Figure 1: Study area on the Tibetan Plateau.

2.2.2. Cross-Wavelet Analysis. To assess the influence of westerly winds and South Asian monsoon on ASMB, the cross-wavelet power spectrum (XWT) and the cross-wavelet coherence spectrum (WTC) were analyzed [44, 45]. The XWT can be defined using the two times series X and Y, with wavelet transforms $W_n^X(s)$ and $W_n^Y(s)$, where n is the time index and s is the scale:

$$W_n^{XY}(s) = W_n^X(s)W_n^{Y^*}(s), \tag{4}$$

where $W_n^{Y^*}(s)$ is the complex conjugate of $W_n^Y(s)$. The XWT can reflect two sequences with the same energy spectral region after wavelet transform, thereby revealing the significance of the interaction between two sequences in different frequency domains.

The WTC is defined as

$$R_n^2(s) = \frac{\left|S\left(s^{-1}W_n^{XY}(s)\right)\right|^2}{S\left(s^{-1}\left|W_n^X(s)\right|^2\right)S\left(s^{-1}\left|W_n^Y(s)\right|^2\right)}, \tag{5}$$

where S is a smoothing operator. The WTC can reflect the coherence range of two wavelet transform in the time-frequency domain.

2.2.3. Westerly Winds Index. The westerly winds index (WWI) in the Northern Hemisphere is based on the Rossby [46] westerly wind index, and it is calculated based on the following equation:

$$\mathrm{WWI} = H_{35} - H_{55}, \tag{6}$$

where H_{35} indicates 35°N at 500 hPa height and H_{55} indicates 55°N at 500 hPa height.

2.2.4. South Asian Monsoon Index. The South Asian monsoon index is calculated using the South Asian monsoon index (SASMI) based on Li and Zeng [47, 48]:

$$\delta_{m,n}^* = \frac{\overrightarrow{V_1} - \overrightarrow{V_{m,n}}}{\overrightarrow{V}}, \tag{7}$$

where $\overrightarrow{V_1}$ is the climate average wind vector for January, $\overrightarrow{V}$ is the climate average wind vector for January and July, and $\overrightarrow{V_{m,n}}$ is the one month (n) in a certain year (m).

3. Results

3.1. Compare the ASMB Definition in the TP. Till date, a considerable amount of research has been dedicated to defining and elucidating the variation of the ASMB. However, there are relatively few relevant studies on TP, and the applicability of these definitions of the ASMB in the TP needs to be discussed further. To this end, we first selected three representative definitions of the ASMB and compared their applicability in the TP (Figure 2). The selected representative boundary definitions include the following: (1) the summer (May–September) 2.0 mm day^{-1} isoline

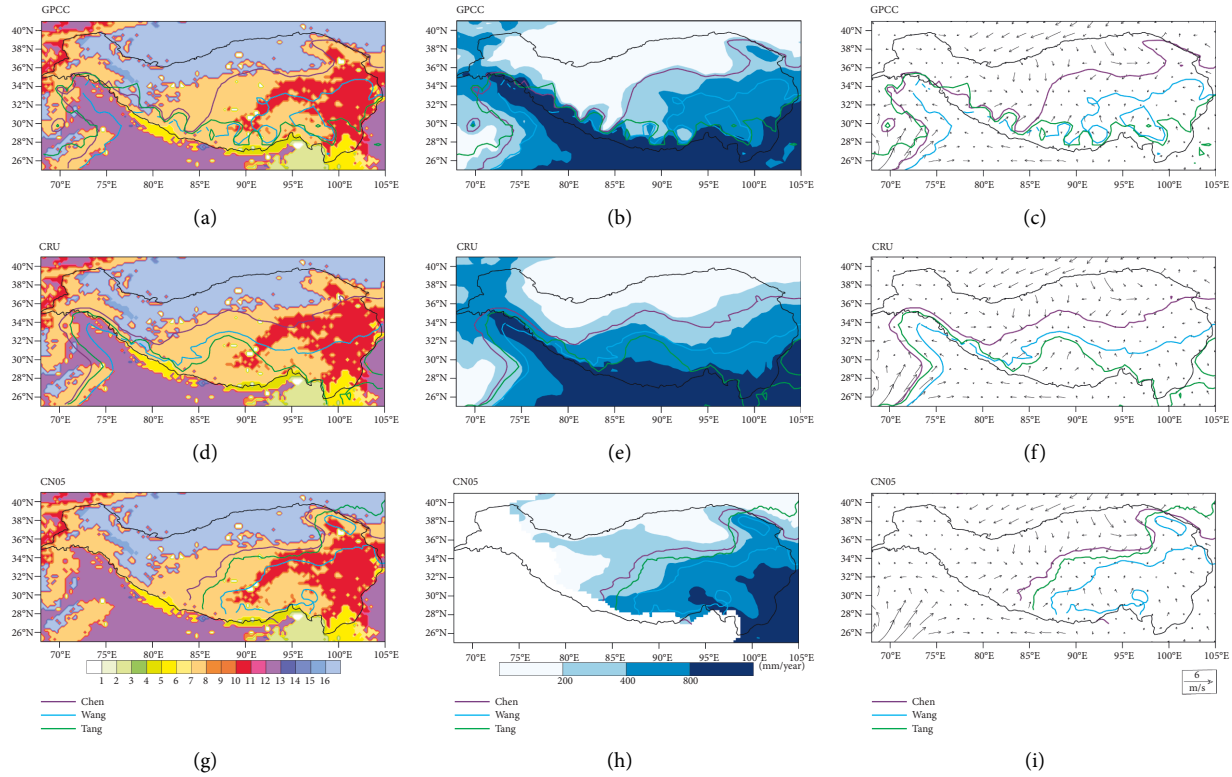

Figure 2: Distribution of modern land cover types, arid-humid zoning map, and surface wind field based on (a–c) GPCC dataset; (d–f) CRU dataset; and (g–i) CN05 dataset. The study area is situated inside the black solid line area. The brown solid line represents the ASMB indicator of 2 mm day^{-1} during summer (May–September) based on Chen et al. [25]. The blue solid line represents the ASMB based on Wang et al. [24]. The green solid line represents the 20 mm isoline of precipitation variance during summer (June–August) based on Tang et al. [23]. The colored areas represent modern land cover types inverted based on MODIS satellite data, where 0 represents water bodies, 1 represents evergreen needleleaf forests, 2 represents evergreen broadleaf forests, 3 represents deciduous needleleaf forests, 4 represents deciduous broadleaf forests, 5 represents mixed forests, 6 represents closed shrubland, 7 represents open shrubland, 8 represents wood savannas, 9 represents savannas, 10 represents grasslands, 11 represents permanent wetlands, 12 represents croplands, 13 represents urban and built-up areas, 14 represents cropland/natural areas, 15 represents permanent snow and ice, 16 represents barren or sparsely vegetated areas, and 17 represents unclassified. In (b) (e) (h), 0–200 mm is defined as the arid zone, 200 mm to 400 mm as the semiarid zone, 400 mm to 800 mm as the semihumid zone, and 800 mm and above as the humid zone [49].

proposed by Chen et al. [25] as the monsoon boundary ("Chen" in Figure 2); (2) the global monsoon index proposed by Wang et al. [24], which is the region in which the difference between the summer (May–September) and winter (November–March of the next year) precipitation exceeded 2.0 mm day^{-1}, and summer precipitation exceeded 55% of total annual precipitation ("Wang" in Figure 2); and (3) the monsoon boundary proposed by Tang et al. [23], as the 20 mm isoline of variance in summer precipitation from June to August ("Tang" in Figure 2).

Figure 2 shows that the three indicators are roughly in the southwest-northeast direction. However, there are also significant differences among these three indicators. For instance, the position of the indicator "Chen" is more northward than the other two indicators, the indicator "Tang" is the more southerly, and the indicator "Wang" is located between the other two. The land cover types in northern TP are barren and sparsely vegetated, with central and southeast TP being dominated by open shrublands and grasslands, respectively (Figure 2(a)). The position of the ASMB indicator "Chen" is located between sparsely vegetated areas, open shrublands, and grasslands; the indicator "Wang" crosses from open shrublands and grasslands; and the indicator "Tang" is located to the south of open shrublands and grasslands. The land cover types are more influenced by climatic conditions and also more sensitive in monsoon boundary areas [50–52]. The fluctuations of the indicator "Chen" generally better reflect the spatial distribution of modern land cover types in the TP. In the arid-humid zoning map, which is divided based on annual average precipitation (Figure 2(b)) [49], the entire TP is roughly divided into arid (north), semiarid and semihumid (center), and humid areas (south). Figure 2(b) shows that the fluctuations of the indicator "Chen" essentially match the spatial distribution of the dividing line of arid and semiarid areas. However, as the indicators "Wang" and "Tang" are located in the semihumid and humid areas, respectively, such a monsoon boundary is unrealistic for the ASM. As for the surface wind field (Figure 2(c)), the ASMB depicted by indicator "Chen" is located in the northernmost position of the southerly wind, which is more compatible than the fluctuating situation presented by the other two

indicators in the TP. Overall, the indicator "Chen" is better at portraying the fluctuations of ASMB in the TP and more meaningful from a climatic-ecological perspective [52]. Thus, the "Chen" 2 mm day^{-1} precipitation isoline during summer (May–September) was considered for further discussions on the ASMB.

Additionally, we analyzed the differences of the three indicators under different datasets using the CRU (Figures 2(d)–2(f)) and CN05 datasets (Figures 2(g)–2(i)). The results indicated that the three datasets (GPCC, CRU, and CN05) performed differently for the TP. The ASMB generated by the GPCC (Figure 2(a)) and CN05 (Figure 2(g)) datasets is more ecologically related and located at the boundary of sparsely vegetated areas-open shrublands-grasslands. In contrast, the ASMB generated by the CRU dataset (Figure 2(d)) does not correspond well to the modern land cover type map. In the arid-humid zoning map, the ASMB generated by the GPCC (Figure 2(b)), CRU (Figure 2(e)), and CN05 (Figure 2(h)) datasets are at the junction of semiarid and arid areas, and all exhibit good climatological significance. In the surface wind field map, the ASMB generated by the GPCC (Figure 2(c)) and CN05 (Figure 2(i)) datasets has a northerly position but is more southerly for the CRU (Figure 2(f)) dataset.

The CRU and GPCC global gridded land surface precipitation datasets are both widely used. Both datasets are based on observation data collected by global meteorological stations and have long time series (1901–present) and high horizontal resolution ($0.5^\circ \times 0.5^\circ$) [52, 53]. The poorer performance of the CRU dataset can be attributed to the method used to process the data. For instance, in the early years, there was a lack of observation values in the TP; consequently, the climatic average was used instead of actual precipitation data [31, 32, 54]. The CN05 precipitation dataset is based on the latest precipitation data of 2472 stations on the ground in China, compiled by the National Meteorological Information Center. The thin-disk spline method of ANUSPLIN software was used for spatial interpolation to generate monthly precipitation data in China with the latest horizontal resolution of $0.5^\circ \times 0.5^\circ$ from 1961 to 2013 [55]. The CN05 dataset is based on the regional dataset of China and shows only specific changes in the TP of the Chinese region. In general, the position of the ASMB generated by the GPCC dataset was superior in terms of delineating and detecting changes, indicating that is a better indicator of climatic-ecological significance. Subsequent analyses focused on the GPCC dataset.

3.2. Variation in the ASMB in the TP. Based on the GPCC dataset, the ASMB was illustrated from 1980 to 2019 using the indicator of summer precipitation of 2.0 mm day-1 to analyze interannual variability. Figure 3 shows that the ASMB generally exhibits a southwest-northeast trend, and any changes were mainly concentrated in the central region of the TP near the Tanggula Mountains and northeastern portion of the TP near the Qilian Mountains, extending as far north as 36N and as far south as 29N in the center part. Along the western part of the plateau, the ASMB changed minimally, especially at 80°E and primarily fluctuated between 32N and 34N. In the eastern part of the TP, the ASMB fluctuated between 36N and 40N. The fluctuations in the amplitude from west to the east suggested a "small-large-small" fluctuation situation.

When analyzing interdecadal variation in the ASM, Ding et al. [56] proposed that it exhibited interdecadal evolution that was first strong, then weak, and then strong after the 1970s. Figure 4 shows that the main fluctuations in interdecadal variation are concentrated in the central part of the TP over the four decades. Lower fluctuations were observed on the western and eastern sides of the TP, indicating an overall southwest-northeast trend. In the western side of the TP, the position of the ASMB extends as far north as 34°N. In contrast, in central TP, the ASMB extends as far north as 36°N. However, interdecadal variation in the eastern part of the TP is not obvious. Overall, interdecadal variability was low in the 1980s and 1990s (Figures 4(a) and 4(b)), but was large in the central and western parts of the TP in the 2000s and 2010s, where it was primarily concentrated (Figures 4(c) and 4(d)).

On analyzing the interannual and interdecadal variations, it can be observed that the ASMB shows different fluctuation situations in different regions of TP; to better reflect the fluctuation magnitude of ASMB and explore how it fluctuated in the TP from 1980 to 2019, three regions (68°E–80°E, 80°E–95°E, and 95°E–105°E) were delineated (Figure 5), based on the results of the interannual and interdecadal "small-large-small" fluctuations shown from west to east (Figures 3 and 4). For these regions, the temporal variation in the average annual latitude of the ASMB was calculated, and the results indicate that the fluctuation of ASMB was relatively smooth before 2000, gradually increasing after 2000 (Figure 5). In the easternmost region (95°E–105°E), the position of the ASMB was the most northerly as compared to the other regions (Figure 5(a)). In the central region (80°E–95°E), the position of the ASMB fluctuated the most, by up to 2.5° latitude in some years (Figure 5(b)). In the westernmost region (68°E–80°E), the position of the ASMB was the most southerly and had the lowest fluctuation (Figure 5(c)). The overall range in fluctuation was noticeably smaller in the western part of the TP (68°E–80°E). In summary, the fluctuation was primarily concentrated in the central part of the TP (80°E–95°E).

The results of changes in the position of the monsoon boundary were assessed periodically using wavelet analysis (Figure 6), and it was confirmed that the characteristics of the ASMB varied for these three regions. Figure 6(a) shows the existence of a 13a–16a periodic signal during 1998–2016 and a 3a periodic signal during 2003–2015, corresponding to the wavelet variance; Figure 6(b) shows the 3a as the main cycle. Figure 6(c) shows that there are clear periodic signals at 5a, 10a–15a, and 25a. Near the 5a scale, the ASMB exhibits a small cycle change in north-south fluctuations and a clear alternating north-south change. At 10a, it exhibits a more stable periodic variation of the signal and a significant interdecadal variation. At 25a, although there are obvious periodic signal variations, the contours are not closed and are not subject to discussion. The corresponding variance

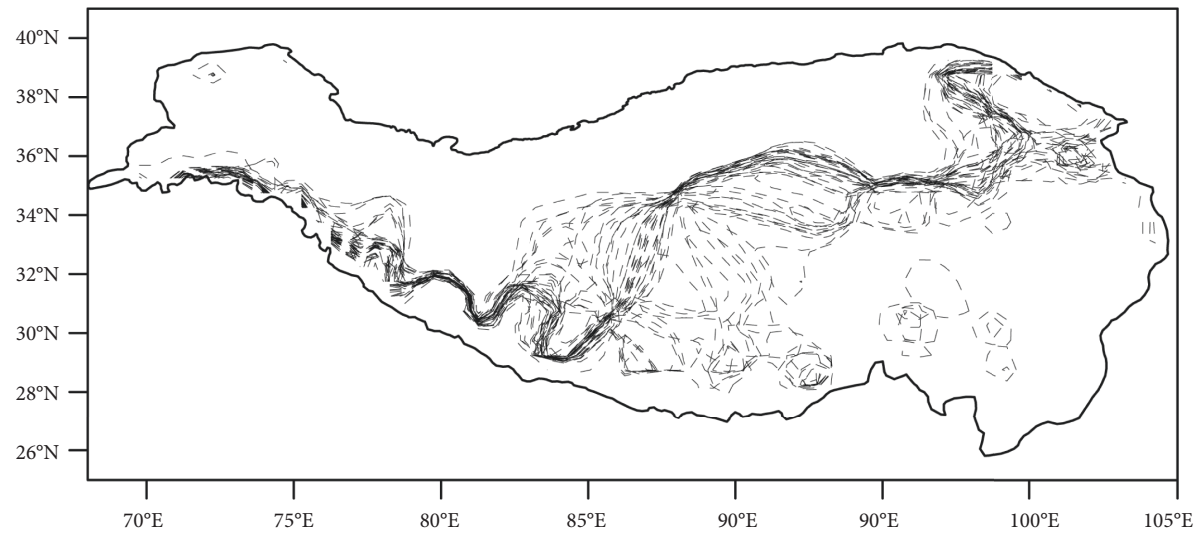

Figure 3: Interannual variation in the monsoon boundary in the TP region during summer. The dotted line represents the location of the boundary for each year between 1980 and 2019.

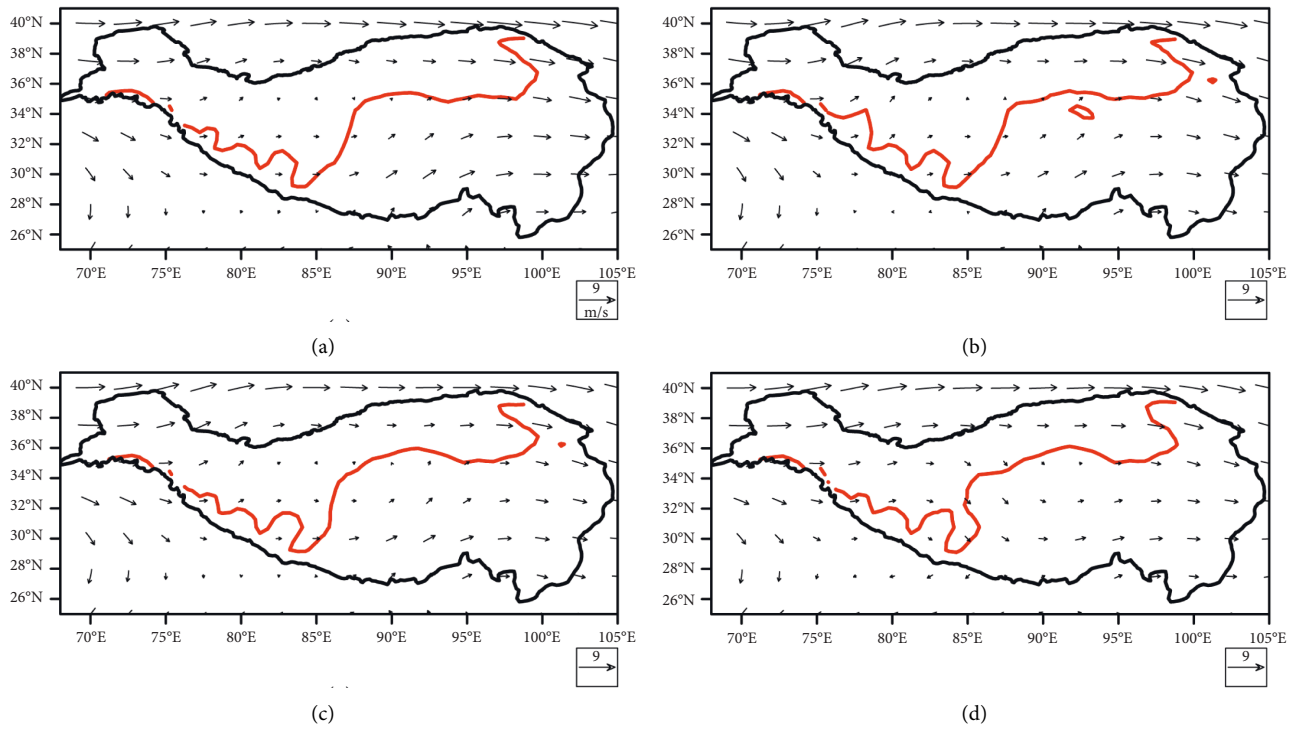

Figure 4: Interdecadal variation in the ASMB and 500 hPa wind field in the TP region during the summer of (a) the 1980s, (b) the 1990s, (c) the 2000s, and (d) the 2010s.

(Figure 6(d)) indicates that 4a and 10a are the first and second cycles, respectively. Figure 6(e)) shows 5a–6a and 14a–15a periodic signals, which mainly occurred in 1993–2019 and 1983–2015. The variance (Figure 6(f)) shows two distinct peaks, which correspond to the 6a and 15a scale periods, with the main cycle occurring at 15a and the second cycle occurring at 6a.

3.3. Cause of the ASMB in the TP. As discussed previously, the ASMB exhibits clear variation in the central part of the TP (80°E–95°E). In this area, there were large fluctuations in the position of the ASMB, with significant interannual variability. Consequently, variation in the position of the ASMB in this region might be a better representative of changes in the entire TP. To elucidate the mechanism

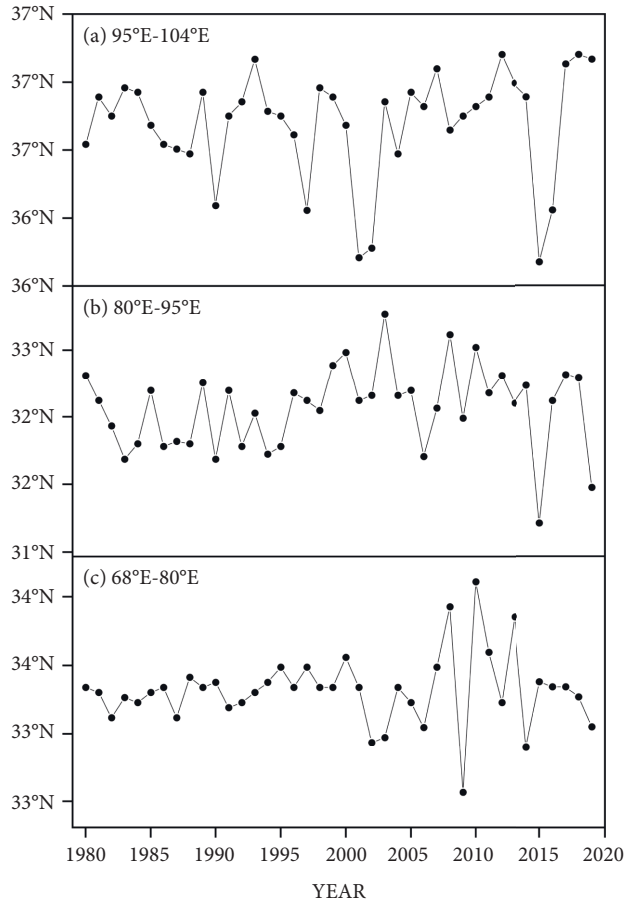

Figure 5: Temporal variations in annual latitude-averaged ASMB for (a) 68°E to 80°E, (b) 80°E to 95°E, and (c) 95°E to 104°E from 1980 to 2019.

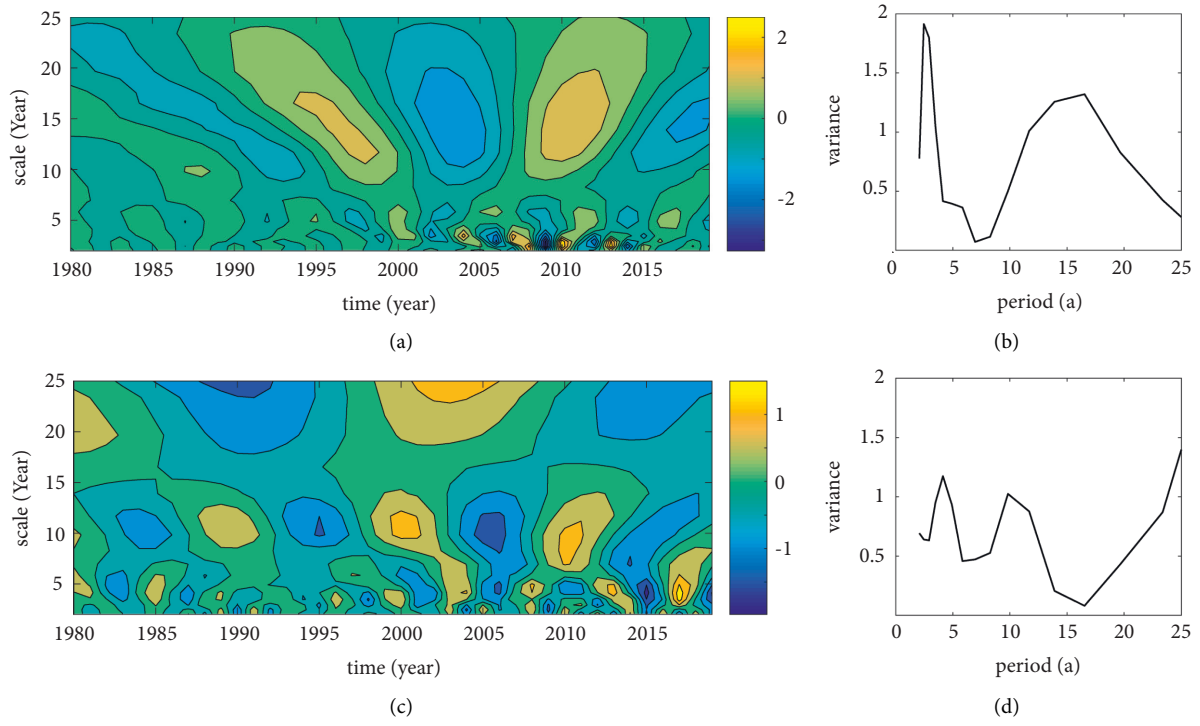

Figure 6: Continued.

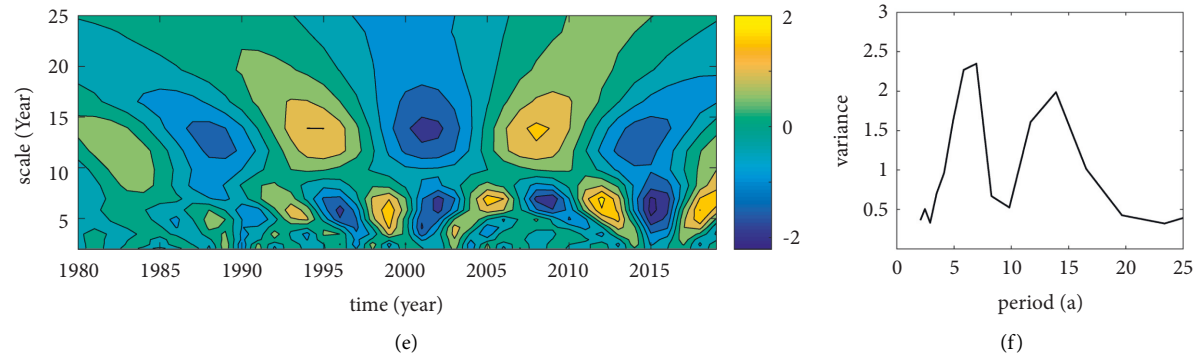

Figure 6: Wavelet analysis plots and its variance of the ASMB in three regions: (a) 68°E to 80°E, (b) 80°E to 95°E, and (c) 95°E to 104°E.

driving this variation, five years, representing the most northerly and southerly years of the ASMB in the TP, were selected in the longitude range from 80°E to 95°E (based on Figure 5). The selected northerly years were 1999, 2000, 2003, 2008, and 2010. The selected southerly years were 1983, 1990, 2006, 2015, and 2019. The 500 hPa wind fields from July to August in the northerly and southerly years were then analyzed individually using composite analysis (Figure 7).

The southern areas of the TP were mainly controlled by the South Asian monsoon (Figures 7(a) and 7(c)), and in northerly years, more areas of the TP were affected, resulting in fluctuations in the ASMB in the TP. The summer wind intensity reflects the characteristics of the main body, and the location of the ASMB reflects the characteristics of the edge [25, 57–59]. In particular, water vapor transport in South Asian monsoons strongly impacts precipitation in the TP (Figure 8). For instance, in a northerly year (Figure 7(b)), there was an anticyclone in the Bay of Bengal, which allowed the South Asian monsoon to affect the regions falling at about 35°N and helped transport warm and humid air to more areas of the TP. This phenomenon caused precipitation to increase in the region and caused the ASMB to shift northward. In a southerly year (Figure 7(d)), there was a strong anticyclone on the west side and a cyclone on the northeast side of the TP. This circulation situation made the westerly winds stronger, which allowed the westerly winds to propagate in the TP and created a situation wherein the South Asian monsoon could only affect the regions falling about 29°N; this reduced water vapor transport, and caused the ASMB in the TP to shift southward.

As shown in Figure 7, the relationship between the water vapor transport of the South Asian monsoon and the location of the ASMB is relatively clear. To examine the water vapor transport problem of the monsoon, two years that had the most northerly and southerly ASMB positions (2003 and 2015, respectively) were selected. Water vapor transport of the entire summer layer in the TP and its surrounding areas was then analyzed (Figure 8): water vapor transport in the TP in summer primarily involved northward zonal transport. There was a strong water vapor transport belt in the Indian Ocean–Bay of Bengal, with a maximum value of 64×10^{-5} kg/(m^{-2}*s). Moisture flowed from the Indian Ocean, through the Indian Peninsula to the Bay of Bengal, and then northward to the TP. It then converted to meridional transport under the influence of the westerly winds. In the northerly years (Figure 8(a)), the center of the water vapor has larger values on the west side of the Indian peninsula. The monsoon transported water vapor along the transport channel up to 32°N or even further north, which might have caused the position of the ASMB to exhibit a significant northward shift. In the southerly years (Figure 8(b)), the meridional transport is deflected at 28°N under the action of strong westerly winds, which might cause a southerly shift in the position of the ASMB.

By analyzing the water vapor flux transport of the monsoon, the effect on the position of the ASMB was elucidated. However, the climate of TP is also influenced by the westerly winds [60, 61]. Therefore, we examined how the westerly winds and South Asian monsoon impact the position of the ASMB (Figure 9). For our investigation, we selected the westerly winds index (WWI) in the Northern Hemisphere, which is based on the index proposed by Rossby [46], and the South Asian monsoon index, which is calculated using the index based on Li and Zeng [47, 48]. The anomaly of the ASMB was then calculated in the TP from 80°E to 95°E; moreover, the anomalies of the westerly wind index (WWI) and SASMI were also calculated (Figure 9).

As we can see in Figure 9, the ASMB changes with the alternation of westerly winds and South Asian monsoon. During strong westerly winds and weak South Asian monsoon years (e.g., 1982, 1990, 1994, and 2016), the ASMB was positioned further south in the TP (Figure 9). During weak westerly winds and strong South Asian monsoon years (e.g., 1985, 1994, 2001, 2006, and 2017), the ASMB was positioned further north in the TP. During years when the westerly winds and South Asian monsoon were both weak (e.g., 1983, 1992, and 2013) or both strong (1990, 1994), three-position patterns of ASMB were exhibited: a stable state, or a southward or northward deflection, indicating the combined influence of the westerly winds and South Asian monsoon during these periods. During 1980–1995, the South Asian monsoon and westerly winds changed alternately, with this pattern being reflected in the position of the ASMB (Figure 9). During 1996–2008, the ASMB anomaly was positive, and its position was more northerly; during this period, the SASMI anomaly was mostly positive and strongly

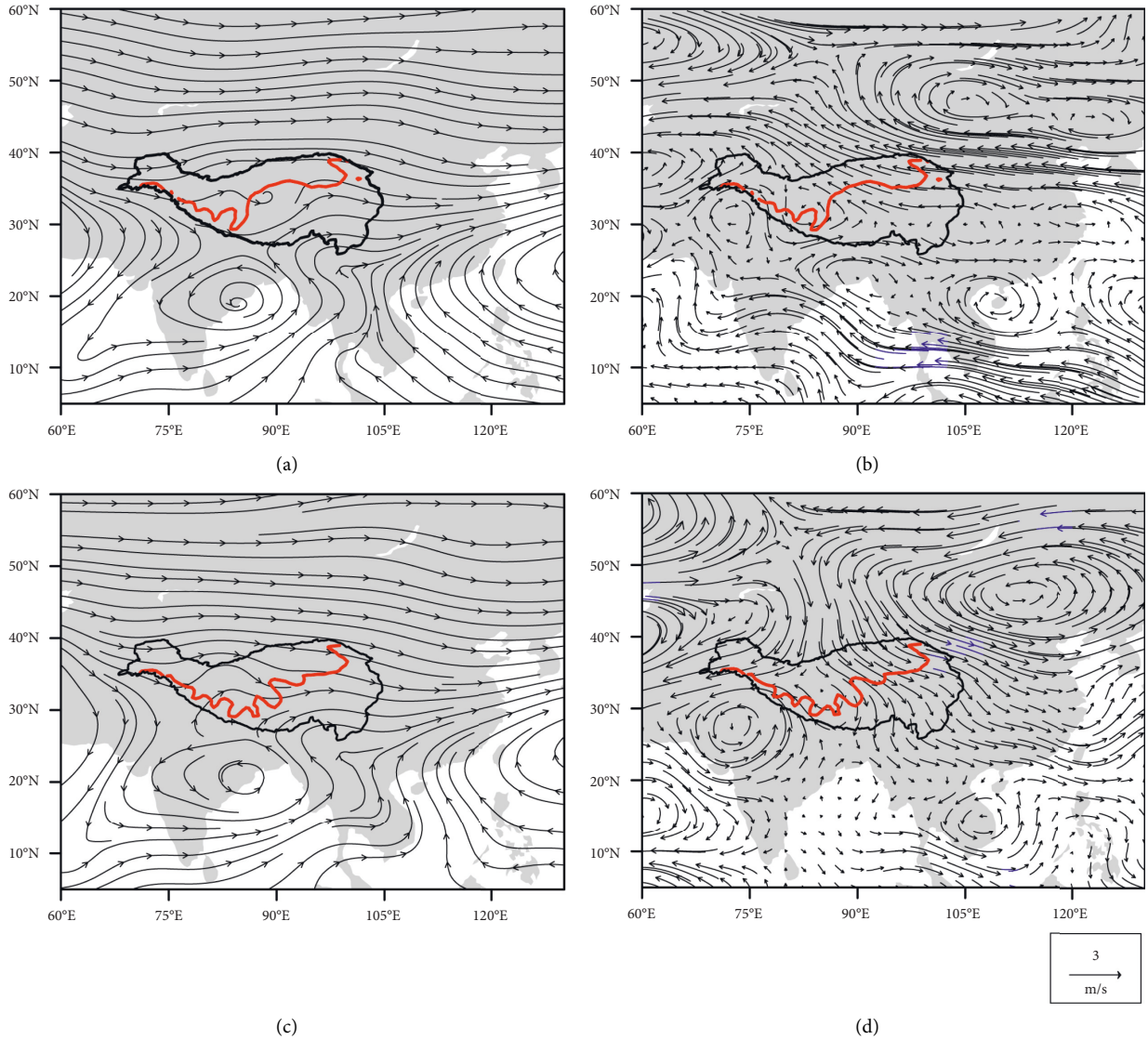

Figure 7: July–August wind vector at 500 hPa in years when the ASMB is in (a) northerly locations and (c) southerly locations. Composite analysis of the wind vectors in years when the ASMB is in (b) northerly locations and (d) southerly locations. The black solid line represents the study area. The red solid line represents the ASMB during northerly and southerly years. Blue vectors represent the 95% confidence level that has been passed.

fluctuated, whereas the WWI anomaly weakly fluctuated. However, there were still such periods when the South Asian monsoon (westerly winds) was strong, and yet changes to the westerly winds (South Asian monsoon) affected the position of the ASMB, which shifted to the south when the westerly winds (South Asian monsoon) became stronger, and to the north when the westerly winds (South Asian monsoon) weakened.

To improve our current understanding of the interactions between the westerly winds, the ASMB, and the South Asian monsoon, cross-wavelet analysis was used. According to the power of the cross-wavelet spectrum (Figure 10(a)), the spectral energy of the ASMB-westerly winds was concentrated in 1-2 a (2005–2008) and 9–11 a (1994–2003) cycles. The spectral energy of the ASMB-South Asian monsoon was concentrated in a 3–5 a (2013–2019) cycle (Figure 10(c)). However, we estimated the significance level for each scale only using values outside the COI [62]. According to the cross-wavelet coherence spectrogram, there were positive (1995–2000) and negative (2003–2006) correlations between the westerly winds and the ASMB (Figure 10(b)). The phase angle indicates that the westerly winds lagged behind the ASMB. For the cross-wavelet coherence spectrogram of the South Asian monsoon-ASMB (Figure 10(d)), negative (1995–2004) and positive (2010–2014) correlations were also observed. In summary, the phase difference between the westerly winds and the South Asian monsoon may indicate the impact of a synergistic effect, which could be amplified by interactions between the westerly winds and the South Asian monsoon.

Based on the calculation results of the cross-wavelet analysis, there may exist a synergistic effect between the

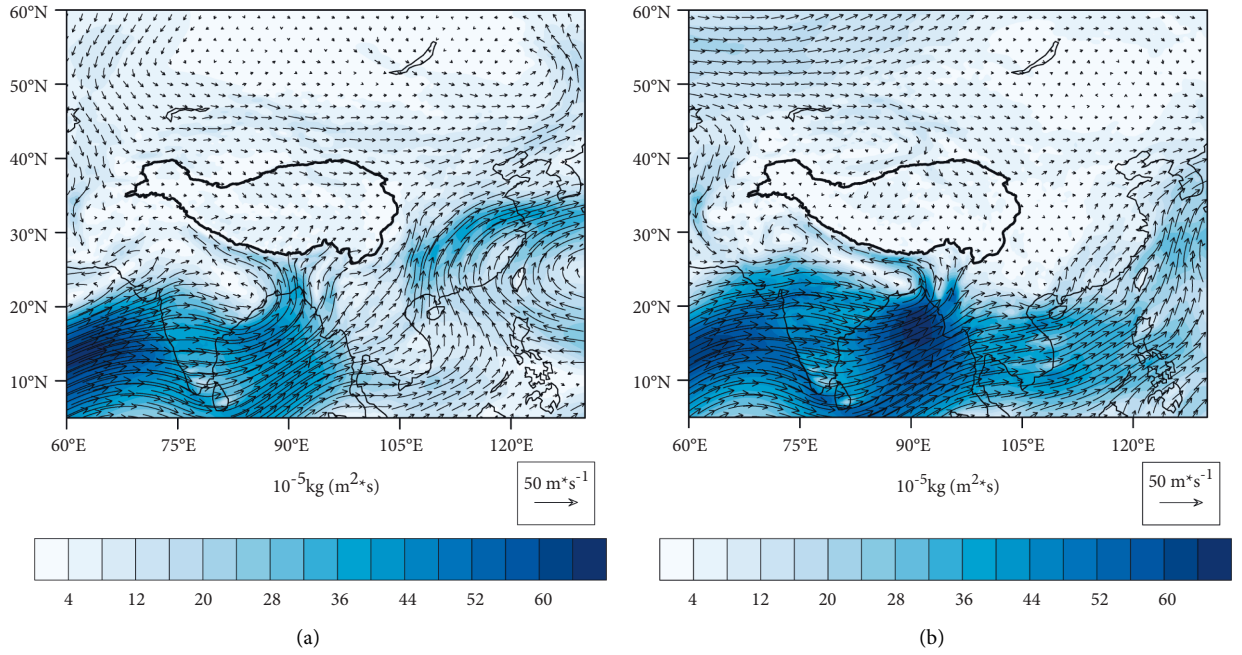

Figure 8: Water vapor flux during summer (1000 hPa~300 hPa) in years during which the monsoon boundary is (a) northerly and (b) southerly. The black line represents the study area.

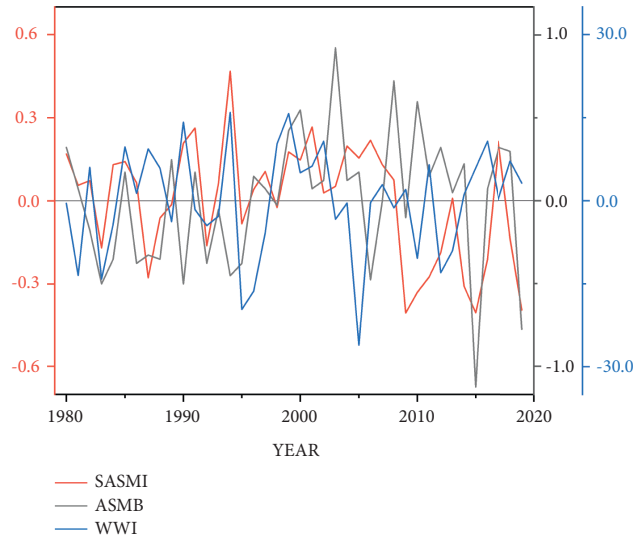

Figure 9: Time series of the ASMB anomaly, WWI anomaly, and SASMI anomaly from 1980 to 2019. The blue solid line indicates the WWI, the black solid line indicates the ASMB, and the red solid line indicates the SASMI.

westerly winds and South Asian monsoon. To examine this synergistic effect, precipitation anomaly maps for positive South Asian monsoon and neutral westerly winds events, neutral South Asian monsoon and positive westerly winds events, positive South Asian monsoon years, and positive westerly winds events were studied (Figure 11); the events with variability exceeding the +1 standard deviation of the SASMI are defined as the positive South Asian monsoon years. Events within +1 and −1 standard deviations for SASMI are neutral South Asian monsoon years [63]. Positive westerly winds and neutral westerly wind years are also defined in this manner. Thus, there are years with positive South Asian monsoon and neutral westerly winds events (1991, 2001, 2006, and 2017), neutral South Asian monsoon and positive westerly winds events (1998, 1999, 2002, and 2016), and positive South Asian monsoon and westerly winds events (1990 and 1994), which impact the position of the monsoon belt differently. In years with positive South Asian monsoon and neutral westerly winds events, the southern part of the TP received more precipitation and the ASMB was more northerly (Figure 11(a)). This positioning reflected the positive phase relationship between the South Asian monsoon and ASMB. During years with neutral South Asian monsoon and westerly winds events (Figure 11(b)),

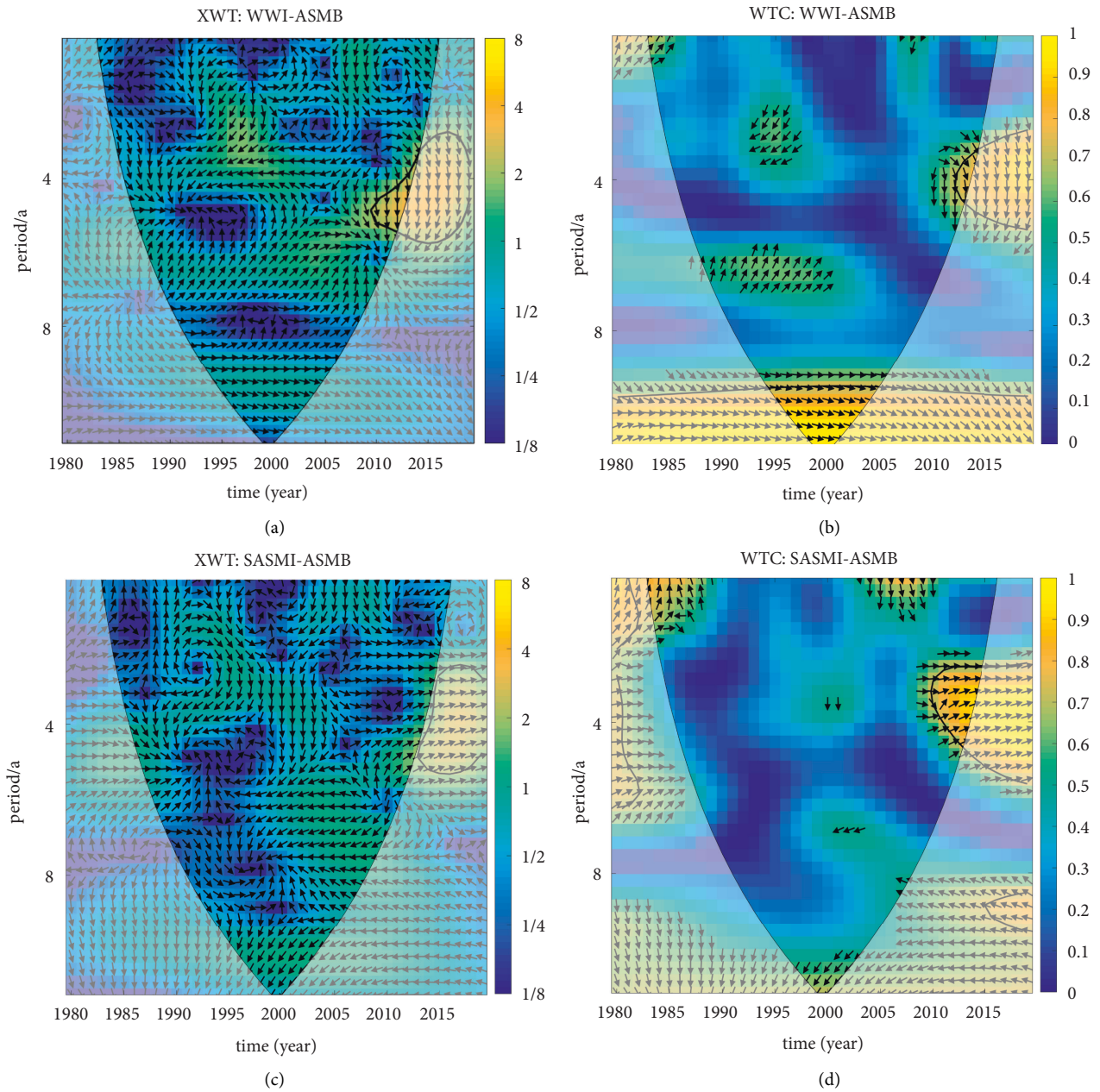

FIGURE 10: Cross-wavelet power spectrum (left) and coherence spectrum (right) of the ASMB with WWI and SASMI from 1980 to 2019. The thick black contour indicates the 95% confidence level against red noise, the cone of influence (COI) where edge effects might distort the picture is shown as a lighter shade.

only the central-eastern part of the TP experienced more precipitation (and the other regions had less precipitation), with the ASMB being more southerly. This phenomenon reflected the inverse phase relationship between the westerly winds and ASMB. However, most of the regions, especially in the center part of TP, did not pass the 95% confident level; consequently, it can be inferred that the precipitation anomalies were not influenced by a single westerly wind or South Asian monsoon. In contrast, in years with positive South Asian monsoon and westerly winds events, a region of low precipitation occurred in the central part of TP, with the ASMB being more southerly (Figure 11(c)). This result indicates that while South Asian monsoon and westerly winds have positive and negative effects on the ASMB, the positioning of the ASMB was influenced by a synergistic effect between the South Asian monsoon and westerly winds.

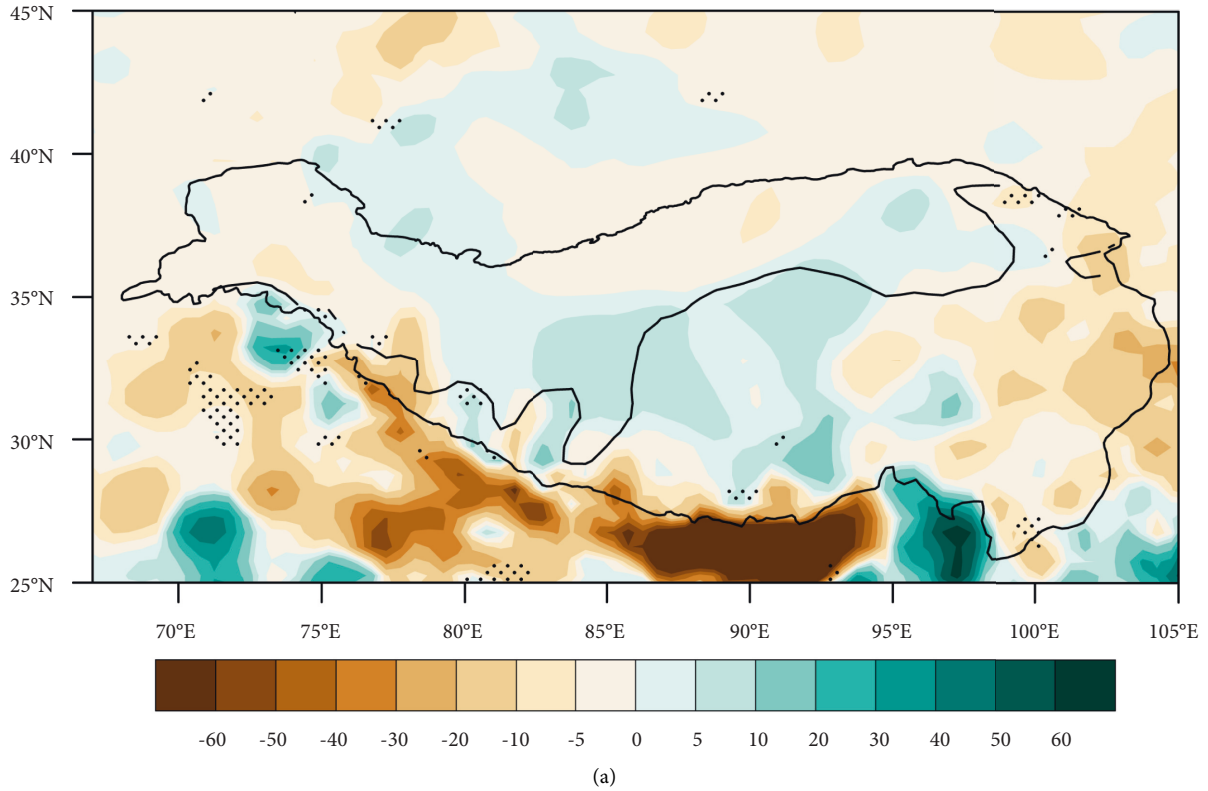

(a)

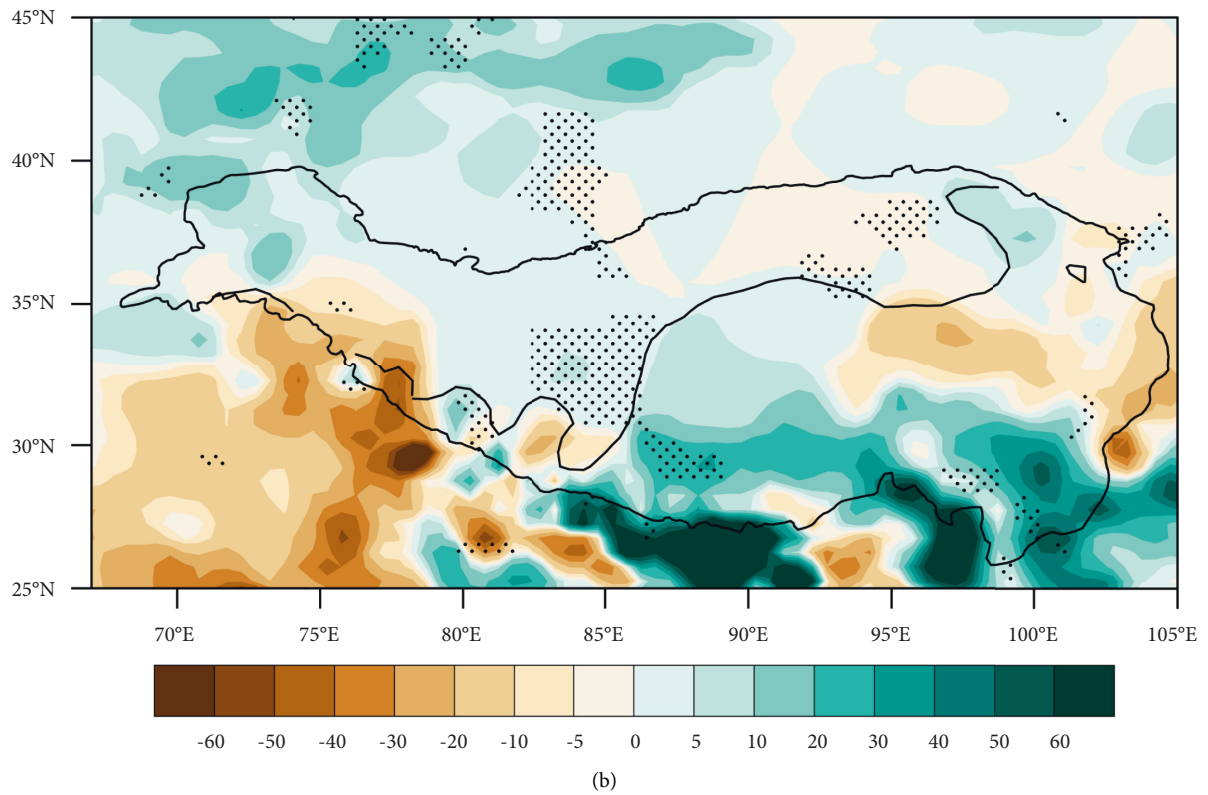

(b)

Figure 11: Continued.

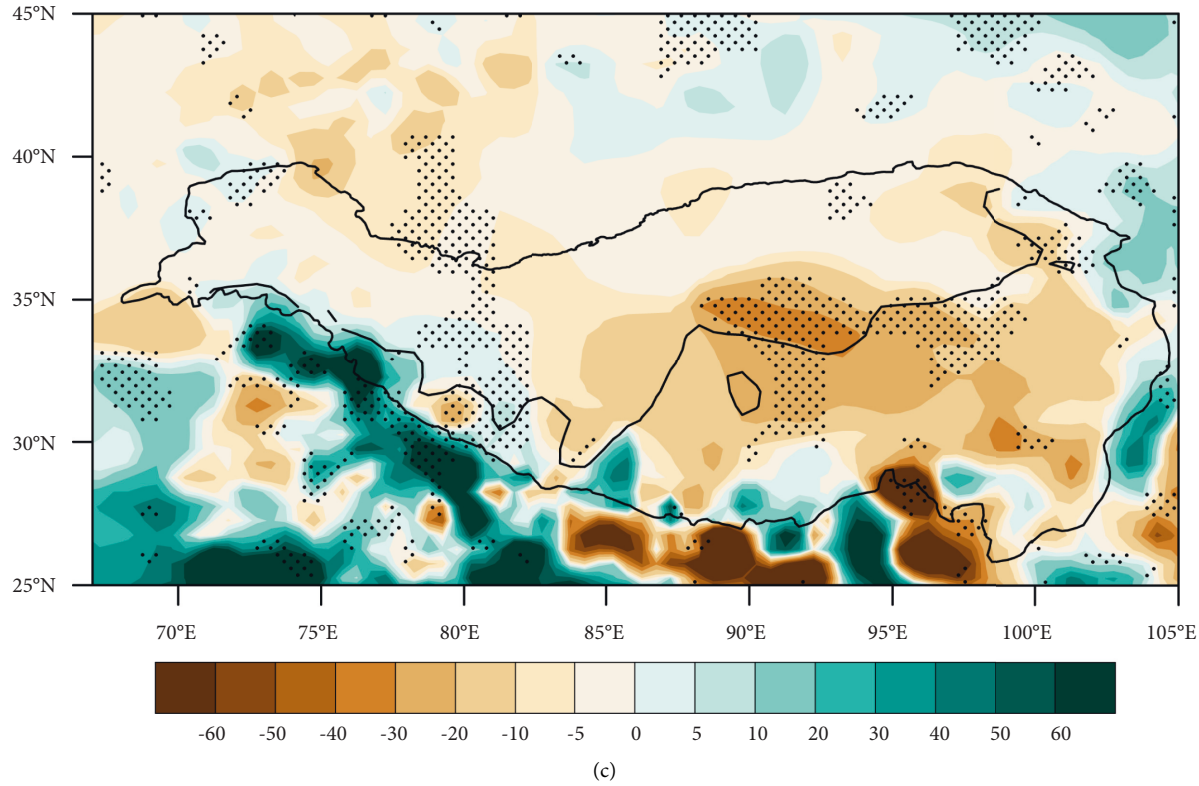

Figure 11: Precipitation anomaly fields for (a) positive south Asian monsoon years and neutral westerly wind years, (b) neutral south Asian monsoon years and positive westerly wind years, and (c) positive south Asian monsoon years and positive westerly wind years. The black dotted area indicates that the 95% confidence level was passed; the black solid line indicates the position of ASMB of the corresponding year.

4. Conclusion and Discussion

Changes in the monsoon affect more than two-thirds of the global population and are of great scientific and social importance [3]. The monsoon system generally has its own variable characteristics [5], the strengths and weaknesses of which are reflected in the variations of their boundaries [19–21]. However, the definitions of different monsoon boundary indices vary considerably, and the performances of these indices are highly uncertain [22–24]. The majority of previous studies have not accounted for the TP, owing to its pronounced topographic effect [26]. In this study, we compared three monsoon indicators and found that the summer (May–September) 2.0 mm day^{-1} isoline proposed by Chen et al. [25] better reflects variations in the ASMB on the TP. We found that this indicator has both climatic and ecological significance by combining modern land cover types, an arid-humid zone map, and the surface wind fields. In addition, we analyzed the effects of water vapor transport from the South Asian monsoon and the action of the westerly winds, for which we observed synergistic effects between the two.

With respect to climate change on the TP, the strength of the monsoon has an impact on precipitation on the plateau [60]. Compared with previous studies [52], we confirmed that the indicator proposed by Chen et al. [25] has climatic and ecological significance, and better reflects the variations in ASMB on the TP. Based on comparisons with the other two datasets, we found that the GPCC dataset is more applicable for the TP [30–32]. The TP is also influenced by the westerly winds [61]. Recent studies have shown that the modulation of the westerlies-monsoon interaction could affect the climate along the monsoon boundary zone [57, 58], and our findings are in accordance with those of previous studies [59]. These findings improve our understanding of the monsoon activity patterns and climate change on the TP. However, this study only examined data from four decades, owing to the limited timescales of the datasets. Modern land cover types were used to verify the ASMB. It is also difficult to obtain reliable vegetation data that spans longer timescales. Our analysis indicates that the ASMB was affected by a synergistic effect between the South Asian monsoon and the westerly winds. The nature of these interrelated mechanisms should be explored further in future research.

Variations in ASMB on the TP were examined using datasets that span four decades. As demonstrated by the interannual and interdecadal results, these variations are concentrated in the central part of the TP region and exhibit a SW-NE trend. Spatial variations in the amplitudes of these fluctuations exhibited a small-large-small trend from south to north. The ASMB is mainly affected by the synergistic effect of the South Asian monsoon and the action of the westerly winds. Further research is required to determine how the monsoon boundary is affected by the relationship between these parameters. The physical mechanisms

involved in this relationship, as well as changes that occur over longer timescales, also require further investigation.

Data Availability

The GPCC dataset can be downloaded from the Global Precipitation Climatology Centre (https://www.cgd.ucar.edu). The CRU dataset can be downloaded from the Climate Research Unit (https://crudata.uea.ac.uk/cru/data). The CN05 dataset can be obtained from the China Meteorological Data Service Centre (https://data.cma.cn). Monthly wind data were obtained from the monthly reanalyzed data of the National Center for Environmental Prediction/Atmospheric Research (https://psl.noaa.gov/data/gridded/reanalysis). The ear5 dataset can downloaded from the Copernicus Climate Change Service (https://www.ecmwf.int/en/forecasts/datasets/reanalysis-datasets/era5). The modern land cover data can be downloaded from the Earth Observing System Data and Information System data center (https://daac.ornl.gov). Boundary data of the Tibetan Plateau were obtained from the National Tibetan Plateau Data Center (https://data.tpdc.ac.cn/).

Conflicts of Interest

The authors declare that they have no conflicts of interest.

Acknowledgments

This research was supported by the Special Survey Project sponsored by the Ministry of Science and Technology of the People's Republic of China (Grant No. 2017FY100903) and the Sichuan Central Government Guides Local Science and Technology Development Project (No. 2021ZYD0019) and the Second Tibetan Plateau Scientific Expedition and Research (STEP) Program (No. 2019QZKK0103).

References

[1] E. Halley, "An historical account of the trade winds, and monsoons, observable in the seas between and near the tropics, with an attempt to assign the physical cause of the said winds," in *Philosophical Transactions of the Royal Society of London*, E. Halley, Ed., vol. 16, no. 183, pp. 153–168, 1986.

[2] G. Hadley, "VI. Concerning the cause of the general trade-winds," *Philosophical Transactions of the Royal Society of London*, vol. 39, 1735.

[3] B. Wang, "Changes in global monsoon precipitation over the past 56 years," *Geophysical Research Letters*, vol. 33, no. 6, 2006.

[4] T. N. Chase, J. A. Knaff, R. A. Pielke, and E. Kalnay, "Changes in global monsoon circulations since 1950," *Natural Hazards*, vol. 29, no. 2, 2003.

[5] T. J. Zhou, B. Wu, and J. Guo, "A review of east Asian summer monsoon simulation and projection: achievements and problems, opportunities and challenges," *Atmospheric Science*, vol. 42, no. 4, pp. 902–934, 2018.

[6] T. J. Zhou, L. X. Zhang, and H. M. Li, "Changes in global land monsoon area and total rainfall accumulation over the last half century," *Geophysical Research Letters*, vol. 35, no. 16, 2008.

[7] Z. X. Han, T. Su, B. C. Huang, T. C. Feng, S. Qu, and G. Feng, "Changes in global monsoon precipitation and the related dynamic and thermodynamic mechanisms in recent decades," *International Journal of Climatology*, vol. 39, no. 3, 2018.

[8] C. P. Chang, K. J. Ha, R. H. Johnson, D. Kim, G. N.-C. Lau, and W. Bin, *Multiscale Global Monsoon System*, The World Scientific Publishing Company, Singapore, 2021.

[9] P. D. Clift, "Asian monsoon dynamics and sediment transport in SE Asia," *Journal of Asian Earth Sciences*, vol. 195, no. 5, 2020.

[10] J. R. Thomson, P. B. Holden, P. Anand, N. R. Edwards, C. A. Porchier, and N. B. W. Harris, "Tectonic and climatic drivers of Asian monsoon evolution," *Nature Communications*, vol. 12, no. 1, p. 4022, 2021.

[11] R. Hamilton, D. Penny, and Q. Hua, "A 4700-year record of hydroclimate variability over the Asian monsoon intersection zone inferred from multi-proxy analysis of lake sediments," *Global and Planetary Change*, vol. 174, no. 5, 2019.

[12] X. T. Sun, Y. H. Ding, and Q. Q. Li, "Interdecadal variation of the atmospheric heat source over the tibetan plateau and surrounding Asian monsoon region: impact on the northern hemisphere summer circulation," *Journal of Meteorological Research*, vol. 35, no. 2, 2021.

[13] Z. M. Ding, G. Huang, F. Liu, and R. Wu, "Responses of global monsoon and seasonal cycle of precipitation to precession and obliquity forcing," *Climate Dynamics*, vol. 6, 2021.

[14] D. Akshay, M. R. H. Kieran, and A. G. Turner, "The four regional varieties of south Asian monsoon low-pressure systems and their modulation by tropical intraseasonal variability," *Weather*, vol. 76, no. 6, 2021.

[15] H. W. Zhang, X. Zhang, Y. J. Cai et al., "A data-model comparison pinpoints holocene spatiotemporal pattern of east Asian summer monsoon," *Quaternary Science Reviews*, vol. 261, no. 3, 2021.

[16] T. H. Ou and W. H. Qian, "Vegetation variations along the monsoon boundary zone in east Asia," *Chinese Journal of Geophysics*, vol. 49, no. 3, 2006.

[17] C. B. Fu, "Potential impacts of human-induced land cover change on east Asia monsoon," *Global and Planetary Change*, vol. 37, no. 3, 2003.

[18] Y. Bai, X. M. Fang, and Q. Tian, "Spatial patterns of soil n-alkane δD values on the tibetan plateau: implications for monsoon boundaries and paleoelevation reconstructions," *Journal of Geophysical Research: Atmospheres*, vol. 117, 2012.

[19] A. Y. Wang, C. S. Wu, W. S. Lin et al., "On the definition of the advance and retreat of the summer monsoon in eastern China," *Plateau Meteorology*, vol. 18, pp. 400–408, 1999, in Chinese.

[20] C. G. Wu, H. S. Liu, and A. Xie, "Interdecadal characteristics of summer wind northward thrust and intensity on summer precipitation in northern China," *Plateau Meteorology*, vol. 24, pp. 656–665, 2004, in Chinese.

[21] P. J. Shi and S. Ha, "Comparison between holocene environmental changes in north China agro-pastoral zone and Africa Sahelian belt," *Earth Science Frontiers*, vol. 9, no. 1, pp. 121–128, 2002.

[22] B. Wang and H. Lin, "Rainy season of the Asian-pacific summer monsoon," *Journal of Climate*, vol. 15, no. 4, pp. 386–398, 2002.

[23] X. Tang, B. D. Chen, and P. Liang, "Definition and features of the north edge of the east Asian summer monsoon," *Journal of Meteorological Research*, vol. 24, no. 1, pp. 43–49, 2010.

[24] B. Wang, J. Liu, H.-J. Kim, J. W. Peter, and S.-Y. Yim, "Recent change of the global monsoon precipitation (1979–2008)," *Climate Dynamics*, vol. 39, no. 5, 2012.

[25] J. Chen, W. Huang, L. Y. Jin, J. H. Chen, S. Q. Chen, and F. Chen, "A climatological northern boundary index for the east Asian summer monsoon and its interannual variability," *Science China Earth Sciences*, vol. 61, no. 1, pp. 13–22, 2018.

[26] Y. X. Sun, S. L. Liu, Y. X. Liu et al., "Effects of the interaction among climate, terrain and human activities on biodiversity on the Qinghai-tibet plateau," *Science of the Total Environment*, vol. 794, 2021.

[27] J. J. Li, S. X. Wen, Q. S. Zhang, F. B. Wang, and B. X. Zheng, "A discussion of the age, magnitude and form of the uplift of the tibetan plateau," *Chinese Science*, vol. 1979, no. 6, pp. 608–616, 1979, in Chinese.

[28] Y. L. Zhang, B. Y. Li, and D. Zheng, "On the extent and area of the tibetan plateau," *Geographical Research*, vol. 1, pp. 1–8, 2002, in Chinese.

[29] U. Schneider, A. Becker, P. Finger, A. Meyer-Christoffer, M. Ziese, and B. Rudolf, "GPCC's new land surface precipitation climatology based on quality-controlled in situ data and its role in quantifying the global water cycle," *Theoretical and Applied Climatology*, vol. 115, no. 1-2, pp. 15–40, 2014.

[30] Y. Xu, X. J. Gao, Y. Shen, C. G. Xu, Y. Shi, and F. Giorgi, "A daily temperature dataset over China and its application in validating a RCM simulation," *Advances in Atmospheric Sciences*, vol. 26, no. 4, 2009.

[31] I. Harris, P. D. Jones, T. J. Osborn, and D. H. Lister, "Updated high-resolution grids of monthly climatic observations—the CRU TS3.10 Dataset," *International Journal of Climatology*, vol. 34, no. 3, pp. 623–642, 2014.

[32] I. Harris, T. J. Osborn, P. Jones, and D. Lister, "Version 4 of the CRU TS monthly high-resolution gridded multivariate climate dataset," *Scientific Data*, vol. 7, 2020.

[33] E. Kalnay, M. Kanamitsu, R. Kistler et al., "The NCEP/NCAR 40-year reanalysis project," *Bulletin of the American Meteorological Society*, vol. 77, no. 3, pp. 437–471, 1996.

[34] J. Munoz-Sabater, E. Dutra, A. Agustí-Panareda et al., "ERA5-Land: a state-of-the-art global reanalysis dataset for land applications," *Journal of Earth System Science*, vol. 13, pp. 4349–4383, 2021.

[35] H. Hersbach, B. Bell, P. Berrisford et al., *Quarterly Journal of the Royal Meteorological Society*, vol. 146, no. 730, pp. 1999–2049, 2020.

[36] M. A. Friedl, A. H. Strahler, J. Hodges et al., *ISLSCP II MODIS (Collection 4) IGBP Land Cover, 2000-2001*, ORNL DAAC, Oak Ridge, TN, USA, 2010.

[37] N. Shi, G. J. Qi, X. X. Huang, J.-X. Liu, and G. Zu, "Significance test and Monte Carlo test used in composite analysis of window field and applications," *Chinese Journal of Atmospheric Sciences*, vol. 28, no. 6, pp. 950–956, 2004, in Chinese.

[38] J. J. Yuan, Z. Y. Ding, and L. Wang, "A statistical study and composite analysis on the characteristics of the extratropical transition of landfall typhoons during 1949–2007," *Journal of Tropical Meteorology*, vol. 27, no. 4, pp. 529–541, 2011, in Chinese.

[39] Y. Lan, "Characteristics of the mean water vapor transport over monsoon Asia," *Advances in Atmospheric Sciences*, vol. 12, no. 2, pp. 195–206, 1995.

[40] R. A. Bryson and R. U. Bryson, "Site-specific high-resolution models of the monsoon for Africa and Asian," *Global and Planetary Change*, vol. 26, no. 1, 2000.

[41] D. S. Pai, L. Sridhar, and M. R. Ramesh Kumar, "Active and break events of Indian summer monsoon during 1901–2014," *Climate Dynamics*, vol. 46, pp. 11-12, 2016.

[42] H. C. Jia and D. H. Pan, "Drought risk assessment in Yunnan province of China based on wavelet analysis," *Advances in Meteorology*, vol. 2016, Article ID 1579415, 10 pages, 2016.

[43] T. Wang, Y. F. Huo, and Y. Luo, "Wavelet analysis of precipitation and solar activity in the central and western Tianshan mountains over the past 300a," *Arid Zone Research*, vol. 33, no. 4, pp. 708–717, 2016.

[44] Y. C. Liu, Z. F. Liu, Y. H. Hao et al., "Multi-time scale characteristics of the runoff in the upstream of rümqi river, Tianshan mountains, based on cross-wavelet transformation," *Journal of Glaciology and Geocryology*, vol. 35, no. 6, pp. 1564–1572, 2013, in Chinese.

[45] T. D. Baddoo, Y. Q. Guan, D. R. Zhang, and A. A.-A. Samuel, "Rainfall variability in the Huangfuchuang watershed and its relationship with ENSO," *Water*, vol. 7, no. 7, pp. 3243–3262, 2015.

[46] C.-G. Rossby, "Relation between variations in the intensity of the zonal circulation of the atmosphere and the displacements of the semi-permanent centers of action," *Journal of Marine Research*, vol. 2, no. 1, pp. 38–55, 1939.

[47] J. P. Li and Q. C. Zeng, "A new monsoon index and the geographical distribution of the global monsoons," *Advances in Atmospheric Sciences*, vol. 20, no. 2, 2003.

[48] J. P. Li and Q. C. Zeng, "A new monsoon index and its interannual variability and relationship with rainfall," *Climate and Environment Research*, vol. 3, pp. 73–87, 2005, in Chinese.

[49] D. Xu, R.-L. Li, and C. H. Wang, "Characteristics of precipitation changes and relationships with water vapour transport in typical arid regions of Asia and Africa under global warming," *Climate and Environment Research*, vol. 21, no. 6, pp. 737–748, 2016, in Chinese.

[50] X. Tang, W. H. Qian, and P. Liang, "Climate characteristics of the summer wind fringe in east Asia," *Plateau Meteor*, vol. 3, pp. 375–381, 2016, in Chinese.

[51] S. R. Zhang, J. L. Xiao, Q. H. Xu et al., "Differential response of vegetation in Hulun lake region at the northern margin of Asian summer monsoon to extreme cold events of the last deglaciation," *Quaternary Science Reviews*, vol. 190, no. 5, 2018.

[52] A. J. Felton, S. Zavislan-Pullaro, and M. D. Smith, "Semi-arid ecosystem sensitivity to precipitation extremes: weak evidence for vegetation constraints," *Ecology*, vol. 100, no. 2, Article ID e02572, 2018.

[53] G. J. Huffman, R. F. Adler, M. L. Morrissey et al., "Global precipitation at one-degree daily resolution from multi-satellite observations," *Journal of Hydrometeorology*, vol. 2, no. 1, pp. 36–50, 2001.

[54] M. G. New, M. Hulme, and P. D. Jones, "Representing twentieth-century space-time climate variability. part II: development of 1901–96 monthly grids of terrestrial surface climate," *Journal of Climate*, vol. 13, no. 13, pp. 2217–2238, 2000.

[55] J. Wu and X. J. Gao, "A gridded daily observation dataset over China region and comparison with the other datasets," *Chinese Journal of Geophysics*, vol. 56, no. 4, pp. 1102–1111, 2013, in Chinese.

[56] Y. H. Ding, D. Si, and Y. J. Liu, "On the characteristics, driving forces and inter-decadal variability of the east Asian summer monsoon," *Chinese Journal of Atmospheric Sciences*, vol. 42, no. 3, pp. 533–558, 2018, in Chinese.

[57] F. H. Chen, J. H. Chen, and W. Huang, "A discussion on the westerly-dominated climate model in mid-latitude Asia during the modern interglacial period," *Frontiers in Earth Science*, vol. 16, no. 6, pp. 23–32, 2009, in Chinese.

[58] F. H. Chen, W. Huang, and L. Y. Jin, "Characteristics and spatial differences of precipitation in arid regions of central Asia under the background of global warming," *Science China Earth Sciences*, vol. 41, no. 11, pp. 1647–1657, 2011, in Chinese.

[59] J. Chen, W. Huang, S. Feng et al., "The modulation of westerlies-monsoon interaction on climate over the monsoon boundary zone in east Asia," *International Journal of Climatology*, vol. 41, 2020.

[60] C. Zhang, Q. Tang, and D. Chen, "Recent changes in the moisture source of precipitation over the tibetan plateau," *Journal of Climate*, vol. 30, no. 5, pp. 1807–1819, 2017.

[61] Y. H. Gao, L. Cuo, and Y. X. Zhang, "Changes in moisture flux over the tibetan plateau during 1979–2011: insights from a high-resolution simulation," *Journal of Climate*, vol. 28, no. 10, pp. 4185–4197, 2014.

[62] A. Grinsted, J. Moore, and S. Jevrejeva, "Application of the cross wavelet transform and wavelet coherence to geophysical time series," *Nonlinear Processes in Geophysics*, vol. 40, no. 11, pp. 561–566, 2004.

[63] L. Jianping, Z. Fei, S. Cheng, F. Juan, and J. Wang, "Pathways of influence of the northern hemisphere mid-high latitudes on east Asian climate: a review," *Advances in Atmospheric Sciences*, vol. 36, no. 9, 2019.